ELSEVIER

Surface Science 440 (1999) 438–450

surface science

www.elsevier.nl/locate/susc

Pressure effects on aluminium oxidation kinetics using X-ray photoelectron spectroscopy and parallel factor analysis

T. Do [a,*], N.S. McIntyre [a,b]

[a] *Surface Science Western, The University of Western Ontario, London, Ontario N6A 5B7, Canada*
[b] *Department of Chemistry, The University of Western Ontario, London, Ontario N6A 5B7, Canada*

Received 11 May 1999; accepted for publication 1 July 1999

Abstract

The effects of water vapour pressure on oxidation kinetics of aluminium have been studied using X-ray photoelectron spectroscopy (XPS) and three-way parallel factor analysis (PARAFAC). While the first technique is a powerful experimental tool for surface oxidation studies, the PARAFAC technique is a sophisticated analytical tool for analysing XPS data. The XPS Al(2p) and O(1s) core level have been used to follow the oxide film growth on clean surfaces at room temperature as a function of oxidation time (ranging from 1 to 60 min) and pressure of water vapour (ranging from 2.0×10^{-6} to 6.5×10^{-4} Pa). The growth of thin oxide films on aluminium surfaces has been found to follow the Cabrera–Mott inverse logarithmic law in all pressure ranges studied. The pressure effects have shown that the defect formation reaction at the oxide film/gas interface is the rate determining process in the aluminium oxidation. The pressure dependence of oxidation kinetics can be explained on the basis of metal vacancies in the defect structure of thin aluminium oxide films.

Keywords: Aluminium oxide; Oxidation; Parallel factor analysis; Surface chemical reaction; XPS

1. Introduction

The structures of thin oxide films on aluminium surfaces are of great interest because of their highly passivating properties, which make aluminium an important material in a wide range of practical applications where corrosion-resistant capability is required. In ambient conditions, the interaction of clean aluminium surfaces with oxygen or water vapour results in a thin amorphous oxide overlayer. However, because of a low oxidation rate and very thin oxide film (<5 nm), use of sophisticated analytical tools is necessary to investigate the oxidation process. Although a number of studies exists on the interaction of aluminium with oxygen and water vapour [1–10], the structure and composition of the oxide film overlayer still remain largely unknown.

The oxidation kinetics of a metal are determined by a number of processes, which fall into two groups: atomic transport through the oxide film, and reactions at one or both interfaces (metal/oxide film and oxide film/gas). The dominant type of defect in the oxide structure defines the mechanism and the direction of the transport process; its concentration determines the oxidation rate. If the rate-determining reaction occurs at the oxide film/gas interface, the oxidation will be a pressure-dependent process, in which the type of defect can be determined from the interfacial reaction. Hence, an investigation of pressure depen-

* Corresponding author. Fax: +1-519-661-3709.
E-mail address: thando@surf.ssw.uwo.ca (T. Do)

0039-6028/99/$ – see front matter
PII: S0039-6028(99)00836-5

dence of oxidation kinetics may provide useful information on the structure of oxide films as well as the oxidation mechanism. For thin aluminium oxide films, earlier works of Cabrera and Mott [11] showed that the oxidation kinetics of aluminium can be described by an inverse logarithmic law. Several later studies [12–20] on the oxidant (CO, O_2 and other gases [12], O_2 [13–19] and H_2O [19,20]) pressure dependence of aluminium oxidation did not, however, lead to a model of oxide film structure which could satisfactorily support the inverse logarithmic law.

In the present work, the growth of a thin oxide film as a result of the interaction of water vapour with clean aluminium surfaces has been studied as a function of exposure time and pressure using the X-ray photoelectron spectroscopy (XPS) technique. The effects of exposure time and pressure on the oxide film growth can be separately examined by using the three-way parallel factor analysis (PARAFAC) technique to analyse the experimental XPS data. As a result, a defect model for thin aluminium oxide film has been proposed to explain the pressure dependence of the oxide growth and the observed inverse logarithmic oxidation kinetics. In this model, metal vacancies are the dominant defect in the thin aluminium oxide film, and the defect formation reaction at the oxide film/gas interface determines the oxidation kinetics.

2. Experimental

Polycrystalline aluminium (99.999% purity) was supplied by Alcan Aluminum Ltd., Kingston, Ontario. Specimens were polished to a 0.05 μm Al_2O_3 finish, degreased ultrasonically, and annealed in vacuum (573 K, 30 min). Before exposure to water vapour the sample surface was cleaned in situ by Ar^+ ion bombardment (3 keV, 10 min) with an incident angle off-surface normal of 55° and an ion dose of $\sim 3 \times 10^{14}$ ions cm^{-2}; this is the minimum Ar^+ ion dose estimated to produce satisfactorily clean aluminium surfaces. The surface cleanness was confirmed by the absence of an oxygen O(1s) peak in a high resolution XPS spectrum. Clean surfaces were then exposed to water vapour in a separate custom-designed preparation chamber attached to the XPS spectrometer at pressures ranging from 2.0×10^{-6} to 6.5×10^{-4} Pa through six levels (level number 1 to 6 corresponds to 2.0×10^{-6}, 7.8×10^{-6}, 1.3×10^{-5}, 6.5×10^{-5}, 1.3×10^{-4}, and 6.5×10^{-4} Pa) and exposure times from 1 to 60 min at 15 time levels: every minute from 1 to 10 min, after that for 15, 20, 30, 45 and 60 min. After exposure to water vapour, under ultra-high vacuum (UHV) conditions, the sample was transferred back into the XPS analytical chamber for collecting XPS spectra. All XPS spectra were obtained using a Surface Science Laboratories SSX-100 spectrometer equipped with a monochromatic Al Kα (1486.6 eV) X-ray source; the binding energy scale was calibrated to give an $Au(4f_{7/2})$ photoelectron line position at 83.98 eV. The UHV system of the XPS spectrometer was maintained at a base pressure of 4.0×10^{-7} Pa; the partial pressure of water in the residual gas detected by using a Dycor Electronics quadrupole mass spectrometer was always less than 1.0×10^{-8} Pa, which allows one to keep the aluminium surfaces in the XPS analytical chamber clean for at least 30 min after Ar^+ ion bombardment. The pass energy of the hemispherical analyser was maintained at 50 eV, giving a constant energy resolution of 0.57 eV. The uptake of oxygen on aluminium surfaces, as a result of its interaction with water vapour at room temperature, was monitored by following the changes in intensity of the XPS Al(2p) and O(1s) photoelectron lines. Representative series of XPS Al(2p) and O(1s) spectra obtained after exposing clean aluminium surfaces to water vapour at a pressure of 10^{-6} Pa are shown in Fig. 1. There was no charging effect observed for all thin oxide films grown on aluminium surfaces under the exposure conditions described above [21]. The centroid of the adventitious reference C(1s) peaks was observed at 286.20 ± 0.05 eV, which satisfactorily agrees with values obtained in an earlier round-robin study [7]. A Shirley background subtraction [22] was performed for all spectra as data preprocessing. The PARAFAC method was then used to analyse the XPS Al(2p) and O(1s) spectra. Through the use of PARAFAC analysis, the XPS Al(2p) and O(1s) spectra shapes can be decomposed based on

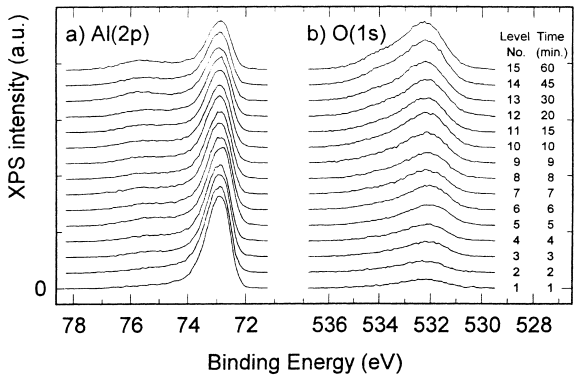

Fig. 1. Representative series of XPS Al(2p) and O(1s) spectra obtained after exposing clean aluminium surfaces to water vapour at a pressure of 2.0×10^{-6} Pa through 15 levels of exposure time from 1 to 60 min.

the variation of peak components through both oxidation time and pressure parameters. The principles of the PARAFAC analysis and its application to analysing XPS spectra are described in detail elsewhere [23].

3. Results and discussion

Exposing the clean aluminium surfaces to water vapour results in growth of an oxide overlayer, which causes not only an attenuation of the photoelectron intensity originating from the metal substrate, but also a shift in binding energy of the photoelectron line aluminium in the underlaying metallic lattice to oxidised aluminium in the overlayer. This gives rise to a new spectral peak in the XPS spectrum, an oxidic component. Increasing exposure time results in a decrease in intensity of the Al(2p) metallic binding energy at 72.80 ± 0.05 eV, and increases of the Al(2p) oxidic component, binding energy at 75.87 ± 0.05 eV, and the O(1s) photoelectron line, binding energy at 532.30 ± 0.05 eV (see Fig. 1).

In the first-principles model [24], the XPS intensity is a multiplicative model, in which the effects of a set of several physically independent variables on the intensity are described as the product of individual effects from each variable. Thus, assuming that the effects of two independent physical variables, such as exposure time t and pressure p, on the photoelectron intensity (of the ith line) can be characterised by two multiplication coefficients or factors f_{ti} and f_{pi}, the XPS intensity affected simultaneously by these two variables, $I_{Z,tp}(E)$, can be expressed as:

$$I_{Z,tp}(E)=\sum_{i=1}^{n} I_{Z,i}(E)f_{ti}f_{pi}+e_{tp}(E) \quad (1)$$

where n is the number of component peaks present in the spectrum, $I_{Z,i}(E)$ is the contribution of the ith component peak from element Z at kinetic energy E, and $e_{tp}(E)$ is the error term. The similarity of Eq. (1) to the mathematical model of the PARAFAC analysis [25,26] is the main grounds for application of this to XPS data. The number of factors in the PARAFAC analysis corresponds to the number of component peaks present in the analysed XPS spectra. By applying the PARAFAC technique to analyse a set of XPS data, one can separately obtain these quantities in Eq. (1): $I_{Z,i}(E)$, f_{ti} and f_{pi} (factor loadings), as a function of kinetic energy E (or equivalent binding energy BE), exposure time t and pressure p, respectively.[1]

Two XPS data matrices were built up from all Al(2p) and O(1s) spectra taken through the ranges of exposure time and pressure studied: one with dimensions of $90\times15\times6$ for Al(2p) data, and the other with dimensions of $94\times15\times6$ for O(1s) data. The PARAFAC analysis on these two data matrices has shown that the XPS Al(2p) and O(1s) spectra can be characterised by three and four factor peaks [21,23], each of which is characteristic of a particular surface reaction process. These results are represented in Fig. 2 and can be summarised as follows. The PARAFAC solution for the Al(2p) data (Fig. 2a–c) has shown that, besides two easily definable single factor peaks, i.e. the metallic at BE of 72.9 eV and the oxidic at BE of 75.8 eV, an additional double-maximum factor peak is found with two components: one at BE of 72.4 eV (Hy) and the other at BE of 75.4 eV (Ox) (see Fig. 2a). The first is identified as due to

[1] The factor loading as a function of kinetic energy E from the PARAFAC analysis is represented further as a factor peak, which may also be decomposed into components, e.g. by curve fitting techniques using 'classical' line shapes.

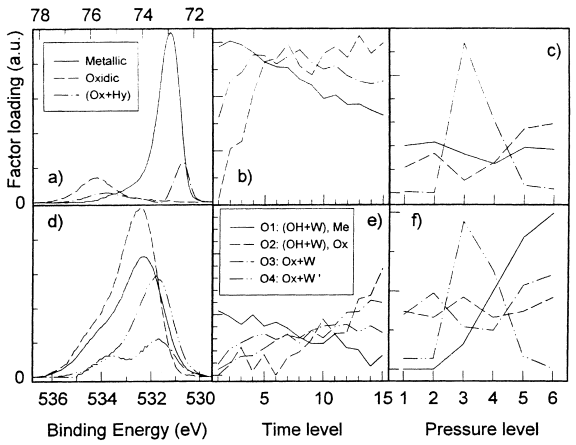

Fig. 2. The PARAFAC solutions for the XPS Al(2p) data (three factor peaks): (a), (b) and (c) and the O(1s) data (four factor peaks): (d), (e) and (f).

interface aluminium hydride, and the second is due to the oxidised aluminium. The assignment of the component at lower BE to an aluminium hydride is based on theoretical work of Gupta and Burger [27], and experimental work of Paul and Hoffmann [28] as well as others [29–32]. The associated component at higher BE has been concluded to be an oxidised form of aluminium based on analysis of peak areas combined with a reaction which relates it to the hydride component. These identifications are supported by the changes in factor loadings as a function of exposure time and pressure (Fig. 2b and c); detailed discussions are presented in Ref. [23]. PARAFAC analysis of O(1s) data (Fig. 2d–f) has shown that all factor peaks in the PARAFAC solution have a dual functionality: an oxide (Ox) or hydroxide (OH) component at a lower binding energy and a hydrate component (W or W′) at higher binding energy (Fig. 2d). The identifications of these components are based on a number of experimental works [4,10,33] and considerations of possible reactions [21], in which these components are involved to give an observed peak association (dual functionality). As an example, the component Ox found at a BE of 531.7_8 eV, in both O3 and O4 factor peaks, is likely due to oxygen in an aluminium oxide lattice as proposed by McCafferty and Wightman [10]; the component W in factor peaks O1, O2 and O3 assigned as due to oxygen in a water molecule is located at a BE of 533.8_5 eV, which is close to the value observed by Szalkowski [4]; the BE position (532.3_6 eV) of the component OH in O1 and O2 factor peaks is found to be close to the value reported for XPS (O1s) peaks for some aluminium hydroxides [33]. Changes in the factor loading of these components as a function of exposure time and pressure (Fig. 2e and f) have established that several surface processes are occurring during the interaction of water vapour with aluminium surfaces [21]: (1) the interaction of OH with the metal surface; (2) the conversion of OH to lattice oxygen and the subsequent oxide nucleation and growth; and (3) the incorporation of OH groups into this oxide lattice. The chemisorbed OH groups on metal surfaces characterised by factor peak O1 [O1: (OH+W), Me; Fig. 2d] show a strong pressure dependence (Fig. 2f). By contrast, the incorporation of OH groups into oxide lattice, which is described by factor peak O2 [O2: (OH+W), Ox; Fig. 2d], is a pressure independent process. The association of OH groups with water molecules in two factor peaks, O1 and O2, is likely due to a recombination reaction of OH groups: $2OH \rightleftharpoons H_2O + O$, which can be used to explain the peak area ratios between these two components, measured as 2.1 and 1.9, respectively. Also, the associated water molecules in oxide component peaks are of a different nature. While the water molecule in the factor peak O3 results from an interaction of aluminium with OH groups, the other in the factor peak O4 is related to a reaction between aluminium hydride and OH group. While the preceding conclusions were discussed in a previous paper [21], a much more detailed analysis of the resultant oxide structure has followed further analysis of the data. This is discussed below.

The atomic ratio of oxygen and aluminium atoms in the overlayer can be determined by the ratio of the corrected XPS intensities of oxygen and aluminium photoelectron lines. Using the results of the PARAFAC analysis on both XPS Al(2p) and O(1s) data obtained previously, the atomic ratios between oxygen and aluminium in the oxide overlayer can be calculated for any selected components in the factor peaks. Fig. 3 represents the atomic ratios r for *total* quantities

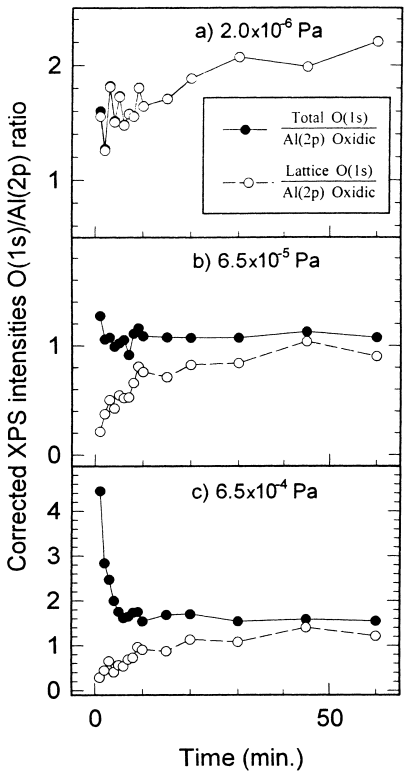

Fig. 3. The corrected XPS intensity ratios between O(1s) and Al(2p) photoelectron lines calculated for selected components in the PARAFAC solutions (see text) for water vapour pressure at: (a) 2.0×10^{-6}, (b) 6.5×10^{-5} and (c) 6.5×10^{-4} Pa.

of oxygen and aluminium atoms measured in the overlayer on aluminium surfaces (filled circles), and for the atomic ratios for oxygen and aluminium that are a discrete part of the lattice[2] structure of the aluminium oxide (open circles) for selected pressures. Oxygen as lattice oxide can be distinguished from hydroxyl and water in the PARAFAC factor peaks O3 and O4 [21].

From Fig. 3, the overlayer grown on aluminium surfaces clearly shows different oxide structures under different pressures of water vapour. It is known that at room temperature the adsorption of water molecules on clean aluminium surfaces is completely dissociative, giving atomic hydrogen and hydroxyl species on surfaces [5]. The latter converts further totally with relative ease through place exchange into an oxide (lattice) oxygen at low flux of impinging water molecules. As a result, under low pressure conditions, the total O/Al ratio reflects that in the oxide lattice (see Fig. 3a). The fact that these ratios are larger than the stoichiometric ratio 1.5 might indicate either an excess of oxygen atoms or a deficiency of aluminium atoms in the oxide overlayer. As shown further in this paper, a detailed analysis of data has proven that the latter is the most possible case because of the presence of aluminium vacancies. As the pressure increases, the conversion of chemisorbed hydroxyl groups to oxygen oxide becomes a rate-determining process, which leads to an accumulation of chemisorbed hydroxyl groups on the metal surface. This corresponds to an increase in factor loading with pressure of the factor peak O1 (see Fig. 2f). Also, such an increase in surface hydroxyl explains the higher total atomic ratios at higher pressure, as seen in Fig. 3b and c; this may result in some participation of the hydrates or hydroxyl groups in bonding in the oxide structure. At middle pressures, where the maximum of interface aluminium hydride is observed (pressure level 3 and 4, Fig. 2c), the obtained atomic ratios are lower than that in bulk Al_2O_3 (Fig. 3b). At higher pressure, the other product of the hydrolysis reaction, i.e. atomic hydrogen, may enter the metal surface as an interstitial hydride; thus, the surface structures formed at higher pressure differ significantly from those at lower pressure.

Assuming the exponential character of the attenuation of photoelectron emerging from a substrate covered by a uniform overlayer with thickness x, the XPS intensities of various component peaks in the XPS Al(2p) and O(1s) spectra can be expressed as follows [34]:

$$I_{\mathrm{Al(Me)}} = I^{\infty}_{\mathrm{Al(Me)}} \exp\left[-\frac{x}{\lambda_{\mathrm{Ox}}(E_{\mathrm{Al,Me}})\sin(\phi)} \right] \qquad (2)$$

$$I_{\mathrm{Al(Ox)}} = I^{\infty}_{\mathrm{Al(Ox)}} \left\{ 1 - \exp\left[-\frac{x}{\lambda_{\mathrm{Ox}}(E_{\mathrm{Al,Ox}})\sin(\phi)} \right] \right\} \qquad (3)$$

[2] The term 'lattice' refers here and further to the primary oxide structure, which is assumed to have a stoichiometric composition of aluminium oxide (Al_2O_3) and does not suggest that the structure is well ordered at an early stage; it could be considered as amorphous.

$$I_O = I_O^{\infty}\left\{1-\exp\left[-\frac{x}{\lambda_{Ox}(E_O)\sin(\phi)}\right]\right\} \quad (4)$$

where $I_{Al(Me)}$ is the XPS intensity of metallic aluminium atoms from the substrate, $I_{Al(Ox)}$ and I_O are the XPS intensities of oxidised aluminium and oxygen atoms from the overlayer; the superscript index '∞' on the right-hand side of the intensity terms denotes the corresponding intensities from pure aluminium metal or oxide; $\lambda_{Ox}(E_{Al,Me})$, $\lambda_{Ox}(E_{Al,Ox})$ and $\lambda_{Ox}(E_O)$ are the inelastic mean free paths (IMFP) of metallic aluminium Al(2p), oxidic aluminium Al(2p) and oxygen O(1s) photoelectron, respectively, in the oxide overlayer with relevant kinetic energies $E_{Al,Me}=1416.9$ eV, $E_{Al,Ox}=1414.0$ eV and $E_O=957.4$ eV; ϕ is the electron take-off angle with respect to the sample surface (35°). These XPS intensities of pure aluminium metallic and oxide are given as: $I^{\infty}_{Al(Me)}=n_{Al(Me)}\lambda_{Me}(E_{Al,Me})K/SF_{Al}$, $I^{\infty}_{Al(Ox)}=n_{Al(Ox)}\lambda_{Ox}(E_{Al,Ox})K/SF_{Al}$ and $I^{\infty}_{O}=n_O\lambda_{Ox}(E_O)K/SF_O$; where the atomic concentrations of aluminium atoms in metal, aluminium atoms in oxide and oxygen atoms in oxide respectively are $n_{Al(Me)}=d_{Me}N_A/M_{Al}$, $n_{Al(Ox)}=d_{Ox}N_A/(M_{Al}+rM_O)$ and $n_O=d_{Ox}N_Ar/(M_{Al}+rM_O)$; d_{Me} and d_{Ox} are densities of aluminium metallic and oxide; N_A is Avogadro's number; M_{Al} and M_O are molar masses of the elements aluminium and oxygen; r is the O/Al stoichiometric ratio; $\lambda_{Me}(E_{Al,Me})$ is the IMFP of aluminium metallic Al(2p) photoelectron in aluminium; SF_{Al} and SF_O are the sensitivity factors of Al(2p) and O(1s) photoelectron lines, 2.49 and 0.60, respectively; and K is an instrumental parameter. Assuming $\lambda_{Ox}(E_{Al,Me})\approx\lambda_{Ox}(E_{Al,Ox})$, a combination of Eqs. (2) and (3) provides the following equation for the thickness of oxide overlayer x:

$$x=\lambda_{Ox}(E_{Al,Me})\sin(\phi)\times\ln\left[\frac{d_{Me}(M_{Al}+rM_O)}{d_{Ox}M_{Al}}\frac{\lambda_{Me}(E_{Al,Me})}{\lambda_{Ox}(E_{Al,Ox})}\frac{I_{Al(Ox)}}{I_{Al(Me)}}+1\right]. \quad (5)$$

In Eq. (5), there are three quantities, which cannot be directly measured, the density d_{Ox} of the oxide overlayer, the IMFP of photoelectrons in the oxide, $\lambda_{Ox}(E_{Al,Me})$ or $\lambda_{Ox}(E_{Al,Ox})$, and the stoichiometric ratio r; in the literature these are usually assumed (r and d_{Ox}) or estimated based on secondary measurements (IMFPs). From Eq. (5), using parameter values presented in Table 1 Strohmeier [36] derived a formula for calculating the oxide thickness on aluminium surfaces. It should be noted that in Strohmeier's formula the oxide overlayer is assumed to be in the form of γ-Al_2O_3, in which the atomic ratio r is 1.5. Further, dividing both sides of Eqs. (2) and (4), and substituting the oxide thickness x from Eq. (5) leads to the following equation:

$$\frac{R_O}{r}=R_{SF}R_\lambda R_{Al}+\frac{R_{SF}dL}{R_M}\times\left[1-\left(\frac{R_MR_\lambda}{dL}R_{Al}+1\right)^{1-1/R_\lambda}\right] \quad (6)$$

where R_O and R_{Al} are the ratios of XPS intensities, $R_O=I_O/I_{Al(Me)}$ and $R_{Al}=I_{Al(Ox)}/I_{Al(Me)}$; R_{SF} is the ratio of sensitivity factors, $R_{SF}=SF_O/SF_{Al}$; R_λ is the ratio of IMFPs, $R_\lambda=\lambda_{Ox}(E_O)/\lambda_{Ox}(E_{Al,Me})$; $dL=d_{Ox}\lambda_{Ox}(E_O)$ and $R_M=\lambda_{Me}(E_{Al,Me})(M_{Al}+rM_O)/M_{Al}$. As mentioned above, increasing exposure time results in growth of an oxide overlayer, which causes an attenuation of the metallic Al(2p) photoelectron signal from the substrate, i.e. a decrease of quantity $I_{Al(Me)}$. The corresponding increase in the oxygen uptake on aluminium surfaces results in an increase of the O(1s) photoelectron intensity, represented by I_O, as well as an increase in intensity of the oxidic component in the Al(2p) spectrum, represented by $I_{Al(Ox)}$. Then, the ratio R_O essentially represents the quantity of oxygen atoms present in the overlayer and the ratio R_{Al} represents growth

Table 1
Parameter values used in the literature for calculating oxide film thickness on aluminium surfaces

	Density (g cm^{-3})	IMFP (nm)
Aluminium metal	2.70 [35]	2.20[a] Al(2p) 2.58[b] Al(2p)
Aluminium oxide	3.5[a]–3.9 (for γ-Al_2O_3) [35]	2.40[a] Al(2p) 2.82[b] Al(2p) 2.09[b] O(1s)

[a] Values used by Strohmeier [36], r assumed to be 1.5.
[b] Values calculated from Tanuma et al. [37,38].

of the oxide overlayer on aluminium surfaces; different ratios can be calculated by selecting appropriate components in the previously obtained PARAFAC factor peaks. Now, some interesting conclusions can be drawn from an examination of the ratio R_O/r as a function of R_{Al}. Fig. 4 shows variations of the R_O/r ratios with changes of R_{Al} calculated for two different oxygen quantities: (a) *total oxygen* from the total XPS O(1s) intensity, and (b) *lattice oxide oxygen* from the oxide components in the PARAFAC factor peaks O3 and O4 for three pressures (selected as in Fig. 3); data for the atomic ratio r is taken from Fig. 3. From Fig. 4, it can clearly be seen that a significant amount of oxygen is incorporated as a part of the aluminium oxide network, which increases with growth of the oxide overlayer characterised by R_{Al}. The difference between the two ratios in Fig. 4 is a measure of non-lattice oxygen (i.e. all oxygen atoms not bounded into the primary oxide lattice) in the overlayer, which would be in the form of OH groups or water molecules. The ratio R_O/r calculated for the lattice oxide oxygen seems to change linearly with R_{Al} at the end of its range in each pressure series. Fig. 5 shows these results for all studied pressures, where the solid line represents a regression line in each series. From Eq. (6), if the variation of the second term in this equation with R_{Al} is very small or can be neglected, the relationship between ratio R_O/r and R_{Al} becomes linear, giving the slope of $R_{SF}R_\lambda$. Statistical tests, applied to pairs of slopes, for all pressure series showed that an average slope can be used to characterise the linearity of these six lines in Fig. 5. The average slope, 2.13, yields a value for R_λ, $\lambda_{Ox}(E_O)/\lambda_{Ox}(E_{Al,Me})$, of 0.51. This value is lower than that calculated using data of Tanuma, Powell and Penn (TPP) [37,38], given in Table 1, i.e. equal to 0.74. Such a significant difference in value of R_λ between our experimental estimation and that calculated using the TPP IMFPs could possibly arise from their use of optical data measured on anodically grown thin aluminium oxide films

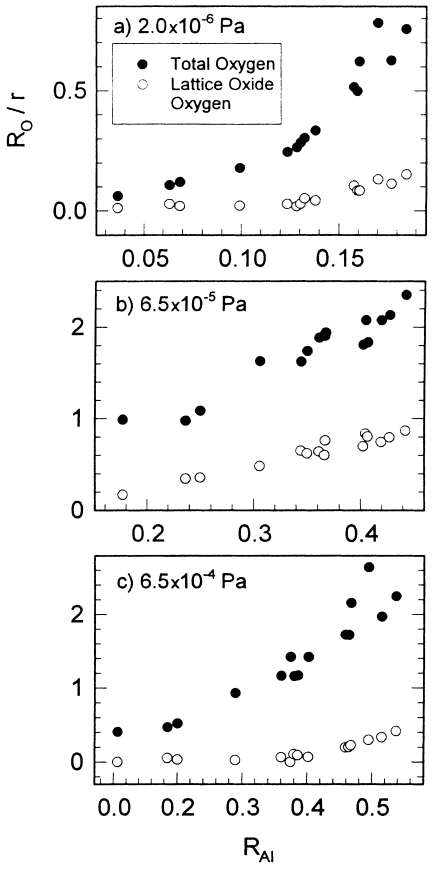

Fig. 4. The ratio R_O/r as a function of R_{Al} for *total oxygen* and *lattice oxide oxygen* (see text) for selected exposure pressures as indicated in Fig. 3.

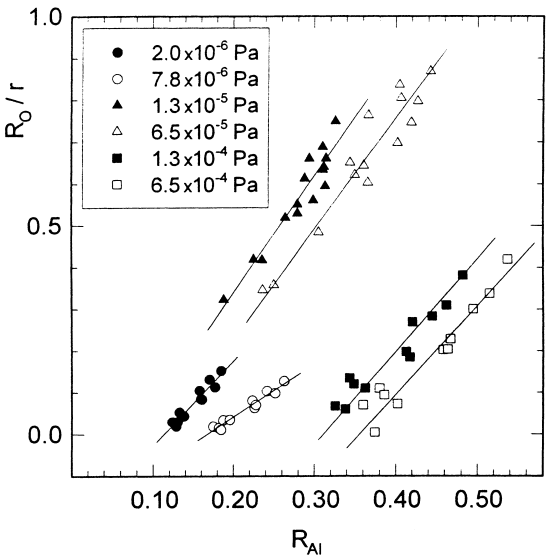

Fig. 5. The ratio R_O/r as function of R_{Al} for *lattice oxide oxygen* for all studied exposure pressures.

[39,40]; the structure of thin anodically grown oxide films may be significantly different from that which grows under our experimental conditions. Thus, the IMFP data given in Table 1 may not be suitable for the case of our thin oxide films. Using the value of $R_\lambda = 0.51$ and a non-linear regression, the other parameter dL in Eq. (6) can be estimated for every pressure series. The obtained best-fit values for dL as a function of pressure are presented in Fig. 6. As suggested from Fig. 6, the parameter dL gradually decreases as pressure increases and becomes constant at high pressure. It should be noted that the variation of parameter dL is affected by both the density of oxide overlayer and the IMFP of O(1s) photoelectron in the oxide layer. Once again, the estimated values of parameter dL are smaller than that calculated using data given in Table 1. From Table 1, assuming the oxide density as for γ-Al_2O_3, 3.5–3.9 g cm^{-3}, and $\lambda_{Ox}(E_O)$ as calculated from TPP [37,38], 2.09 nm, the absolute value of dL can be in the range 7.3–8.2, which is much higher than our estimated value, which varies from 2.0 to 3.4. That means, under any assumption, one or both of the oxide density or $\lambda_{Ox}(E_O)$ are smaller than those given in Table 1, and this suggests that the parameters given in Table 1 may not be valid to characterise the thin oxide films grown on aluminium surfaces in our experimental conditions. In particular, the assumption of stoichiometric oxide (γ-Al_2O_3) for the oxide overlayer on aluminium surfaces leads to, as shown below, the most severe deviation and uncertainty in the estimation of thickness.

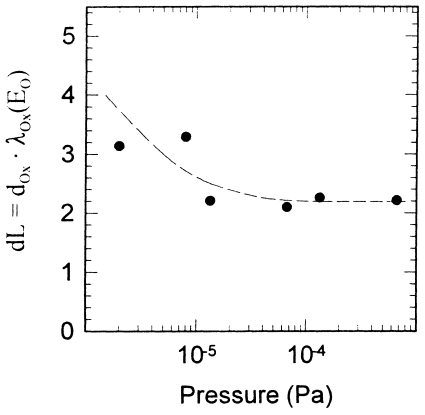

Fig. 6. Estimate of dL as a function of exposure pressure.

Eqs. (2)–(4) show that the thickness of oxide overlayer can be calculated in different ways using our available collected XPS data. In order to eliminate uncertainty due to an assumption for $\lambda_{Ox}(E_{Al,Me})$, and to compare obtained results, a relative thickness x_{rel} was used, which is defined as the ratio of the calculated thickness to the IMFP of Al(2p) photoelectron in oxide, $x_{rel} = x/\lambda_{Ox}(E_{Al,Me})$. The collected XPS data allowed us to calculate the relative thickness by the following four methods.

(A) Two peaks fitted: using two component peaks, the metallic and the oxidic, to fit the original XPS Al(2p) spectra by the curve fitting technique and to obtain the R_{Al} ratios. The assumed data are: the oxide density d_{Ox} and stoichiometric ratio r as assumed by Strohmeier [36]; the IMFPs are of TPP from Table 1. The oxide relative thickness is calculated from Eq. (5).

(B) PARAFAC-derived Al(2p) ratio: using the metallic and the oxidic Al(2p) factor peaks (Fig. 2a) to obtain the R_{Al} ratios. The assumed data are: the oxide density d_{Ox} and the TPP IMFPs (from Table 1); stoichiometric ratios r are taken from data in Fig. 3; calculations of relative thickness are based on Eq. (5).

(C) PARAFAC-derived O(1s) ratio: using the sum of lattice oxide oxygen components from O(1s) factor peaks O3 and O4 (Fig. 2d) and the metallic Al(2p) factor peak (Fig. 2a) to obtain the R_O ratios. The ratio R_O is then used to determine the oxide thickness by a numerical method applied to a combination of Eqs. (2) and (4). The oxide density d_{Ox}, IMFPs and the stoichiometric ratios r are as in method B.

(D) dL estimated: using the R_{Al} ratios calculated as in method B; the oxide relative thickness is calculated from Eq. (5) using the dL value estimated above.

Fig. 7 shows calculation results for the oxide growth as a function of exposure time by using the original XPS data (method A; filled circles) and several independent sets of data provided from PARAFAC analysis (methods B, C and D; filled triangles, open triangles and open rhombs, respectively) for three selected pressures. Although a

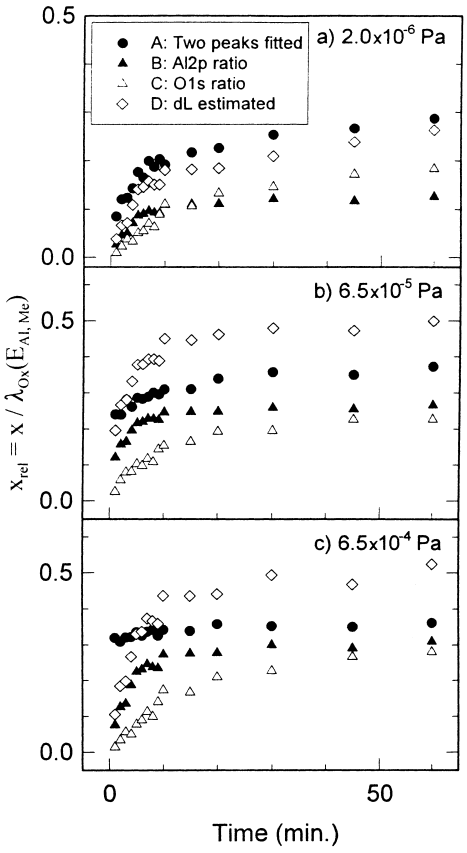

Fig. 7. Relative thickness, x_{rel}, of oxide overlayer calculated by four different methods (see text) as a function of oxidation time t (min) for selected exposure pressures as indicated in Fig. 3.

similar character of the oxide growth is observed for results obtained by methods B, C and D, the use of the assumed data (in methods B and C) results in an overestimation for the oxide thickness compared with the experimentally estimated data (method D). By contrast, the oxide thicknesses estimated by method A provide different results, which can clearly be seen at higher pressure in early stages up to 10 min (see Fig. 7c). This is likely due to assumptions made for parameters used in calculations, the oxide density d_{Ox} and IMFP, as well as to the assumption of stoichiometric ratio for the composition of the oxide overlayer. At lower pressure (Fig. 7a), the oxide thickness calculated from two peaks fitted (method A) varies almost in the same way as that with dL estimation (method D); this is because the assumed atomic ratio (1.5) for the oxide overlayer is close to that observed (see Fig. 3a), particularly at the early stages. In consequence, the two peaks fitted method (method A) can be applied for thickness estimation only under those particular conditions of experiments.

Our previous work [41] showed that the oxidation kinetics of aluminium are best described by an inverse logarithmic law. In this work [41] the effect of water vapour pressure p has been incorporated with the effect of exposure time t in the oxidation kinetics by an exposure parameter, which includes both exposure time and pressure via a product $t \times p$, and has the unit of Langmuirs (1 Langmuir $= 1.33 \times 10^{-4}$ Pa s). As shown above, by using the PARAFAC technique the effects of exposure time and pressure can be separately extracted, which are now used to examine the oxidation kinetics. The rate of oxide growth, theoretically, depends on a flux of ions, J_{ion}, across the oxide overlayer, which can be expressed by a general equation:

$$J_{ion} = -D_i \frac{dc_i}{dx} + c_i v_i \quad (7)$$

where D_i is the diffusion coefficient, c_i is the concentration and v_i is the drift velocity of an ion, which is the diffusing species in the oxide overlayer. The first term in the right-hand side of Eq. (7) is Fick's first law and the other derives from Ohm's law; these describe the motion of an ion or charged species in the oxide overlayer under its concentration gradient dc_i/dx and electrostatic field F, respectively. The electrostatic field, following the Cabrera–Mott theory of low-temperature oxidation [11], is provided by a constant contact potential V created by ionised adsorbed oxygen atoms at the oxide/gas interface. If x is the oxide film thickness, the field strength is given by: $F = V/x$; the drift velocity is proportional to the electrostatic field: $v_i = \mu_i F$, where μ_i is the ion mobility. For very thin oxide films, i.e. x very small, the electrostatic field becomes very strong; e.g. for a film 5 nm thick the field can be of the order of 10^7 V/cm [11]. Under these conditions, the concentration gradient has no effect or can be neglected in the ion flux and the electrostatic field is the only

driving force for ion diffusion. Also, the field is so strong that space-charge effects in the oxide overlayer become negligible; the drift of ions is an exponential function of the field F [11]:

$$v_i = v_i a_{ox} \exp\left(-\frac{U}{k_B T}\right)\left[\exp\left(\frac{q_i a_{ox} F}{k_B T}\right) - \exp\left(-\frac{q_i a_{ox} F}{k_B T}\right)\right] \quad (8)$$

where v_i is the ion jump frequency ($\sim 10^{12}\ s^{-1}$), a_{ox} an interatomic jump distance in the oxide overlayer; U an activation energy for diffusion of an ion species with a charge q_i, and k_B and T are the Boltzmann's constant and temperature, respectively. For very thin oxide films, according to Cabrera and Mott, the field-dependent transport of ions becomes rate-determining in the oxidation process; the electrons are assumed to be transported faster through the oxide film by a number of mechanisms, including quantum tunnelling, impurity conduction or Schottky emission. Thus, using Eqs. (7) and (8) for the condition $q_i a_{ox} F/k_B T \gg 1$, the oxidation rate dx/dt, which is proportional to the ion flux ($dx/dt = \Omega J_{ion}$, where Ω is the volume of oxide per diffusing charged species), is given by:

$$\frac{dx}{dt} = \Omega c_i u \exp\left(\frac{x_1}{x}\right) \quad (9)$$

where u is the jump frequency function, $u = v_i a_{ox} \exp(-U/k_B T)$, $x_1 = q_i a_{ox} V/k_B T$ is the upper limiting thickness below which the validity of the concept of field-driven transport is held. It can be shown that Eq. (9) has an approximate solution:

$$\frac{\Omega c_i u t}{x_1} = \left(\frac{x}{x_1}\right)^2 \exp\left(-\frac{x_1}{x}\right). \quad (10)$$

Following the same assumptions made by Cabrera and Mott, Eq. (10) can be simplified to an approximate form: $1/x = -(1/x_1)\ln(t) +$ constant, which represents the well-known inverse logarithmic law for oxide growth at low temperature. As evidence for the Cabrera–Mott theory, a plot of $1/x$ versus $\ln(t)$ should yield a straight line, which provides a slope $-1/x_1$. Fig. 8 shows

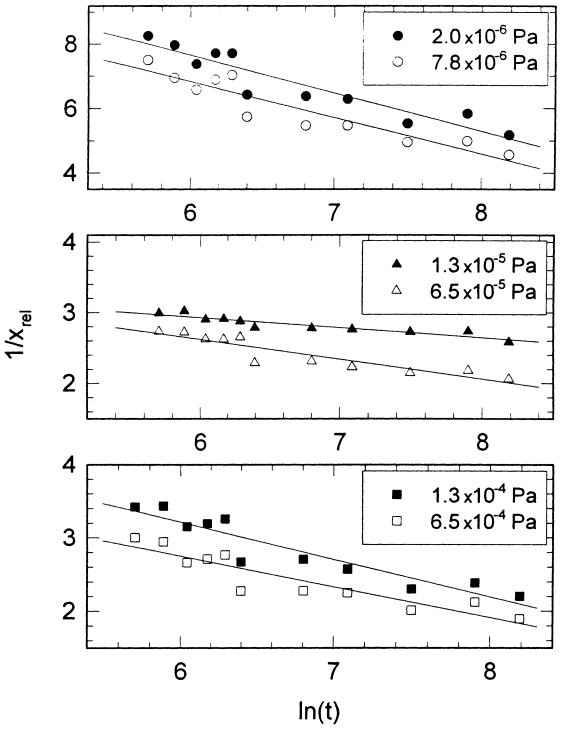

Fig. 8. The relative thickness of oxide films in the form of inverse-logarithmic expression: $1/x_{rel}$ as a function of $\ln(t)$; the x_{rel} calculated by method D (see text) for all studied pressures. The solid lines represent regression lines.

the plots of $1/x$ as a function of $\ln(t)$ for all pressures studied, where the oxide thickness x was replaced by the relative thickness, x_{rel}, calculated from the estimated dL value (method D, Fig. 7). The solid lines in Fig. 8 represent the best-fit lines obtained by linear least-squares regression. These regression lines, with reasonably good correlation coefficients (≥ 0.85), confirm then the inverse logarithmic law for the oxidation kinetics and validity of related assumptions made by theory. On the other hand, the experimental data can be better tested for Eq. (10) by the relation $1/x$ versus $\ln(t/x^2)$. This is because Eq. (10) can be rewritten as:

$$\frac{1}{x} = \frac{1}{x_1}\ln\left(\frac{1}{\Omega c_i u x_1}\right) - \frac{1}{x_1}\ln\left(\frac{t}{x^2}\right). \quad (11)$$

Eq. (11) shows that a plot of $1/x$ versus $\ln(t/x^2)$ should yield also a straight line with the

same slope $-1/x_1$ as the plot $1/x$ versus $\ln(t)$. Fig. 9 shows the same data from Fig. 8 plotted as $1/x$ versus $\ln(t/x^2)$, also with x replaced by x_{rel}. Once again, the experimental results fall on straight lines as predicted by theory, Eq. (11). Here, the solid lines also represent the best-fit lines from linear regression; the same values for slopes, $-1/x_1$, were obtained as those from the plot $1/x$ versus $\ln(t)$ in Fig. 8, with similar correlation coefficients (≥ 0.85). Although an alternative form of thickness versus $\log(t)$ can be well fitted to these data (also with similar correlation coefficients), the direct logarithmic rate may not be considered as governing oxidation kinetics. This is because, according to Hauffe and Ilschner [42], in the logarithmic oxidation kinetics, the electron transport through the oxide film is the rate-limiting process. This leads to a simple expression for oxide thickness: $x = x_e \ln(t) + \text{constant}$, where x_e is the limiting thickness and can be estimated from the slope of the straight line plotting x versus $\ln(t)$. The limiting thickness can be used to verify the proposed model since in both cases, direct or inverse logarithmic kinetics, it is required that $x \ll x_e$ or $x \ll x_1$. Our calculations show that, in all studied pressures, the thickness data satisfy only the latter condition, thus suggesting the inverse logarithmic is the best mechanism to describe the oxidation kinetics of aluminium.

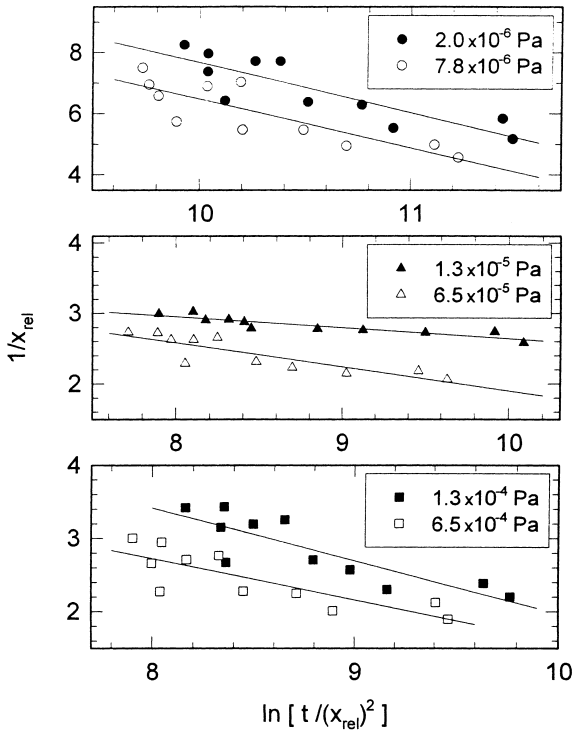

Fig. 9. The relative thickness of oxide films from Fig. 8 re-plotted in the form of Eq. (11): $1/x_{rel}$ as a function of $\ln[t/(x_{rel})^2]$. The solid lines represent regression lines.

As shown above, the pressure effect on oxidation kinetics has been demonstrated in the atomic ratio (Fig. 3) and the *dL* parameter (Fig. 6), which represents the structure of the oxide overlayer on aluminium surfaces. On the other hand, the pressure effects can be examined in more detail by analysing the pressure dependence of the concentration term, c_i, in Eq. (11). From Eq. (7), c_i denotes a concentration of diffusing species in the oxide overlayer. Under an electrostatic field, only a charged species is able to migrate, which can be one of four possible types of ionic defects in aluminium oxide. Using the notation system proposed by Kröger and Vink [43], these defects are: two types of vacancies, aluminium V_{Al} and oxygen V_O, and two types of interstitials, aluminium Al_i and oxygen O_i. For example, consider the case of a constant concentration of metal vacancies in the oxide layer under a certain level of water vapour pressure. In an amorphous network of the aluminium oxide, similar to the crystalline structure, the metal vacancy can be a vacant position of the aluminium atom. Assuming that the 'ideal' amorphous network of the aluminium oxide is stoichiometric, the formation of metal vacancies at the oxide film/gas interface can be described by the following reactions:

$$H_2O(g) + (\text{surface site}) \rightleftharpoons H_2O(ad) \quad (12)$$

$$H_2O(ad) \rightleftharpoons OH(ad) + H(ad) \quad (13)$$

$$3OH(ad) \rightleftharpoons 2V_{Al}''' + 6h^{\cdot} + 3O_O + 3H(ad) \quad (14)$$

where V_{Al}''' and $h^{\cdot}$ are ionised aluminium vacancy and electronic hole, respectively ($V_{AL} \rightleftharpoons V_{Al}''' + 3h^{\cdot}$); ad denotes an adsorbed state. The first two reactions, (12) and (13), describe the adsorption and hydrolysis reactions. It has been suggested by experimental work of Paul and Hoffmann [28], theoretical calculations of Zhukovskii et al. [44]

and confirmed by our previous work [21] that the hydroxyl groups play the role of a precursor in the oxidation process on aluminium surfaces. From Eqs. (12)–(14), using the neutrality condition:

$$[V'''_{Al}] = \tfrac{1}{3}[h^{\cdot}]$$

the concentration of charged defects in the oxide overlayer can be derived as: $c_i = [V'''_{Al}] = A_p p^y$, where A_p is a constant containing the reaction (12), (13) and (14) constants, p is the water vapour pressure, and $y = 3/8$. Substituting c_i and re-arranging Eq. (11) yields:

$$\frac{x_1}{x} - 2\ln(x) = \ln\left(\frac{1}{\Omega A_p u x_1 t}\right) - y\ln(p). \qquad (15)$$

Eq. (15) can be used with the estimate x_1 from the slope of linear regression lines in Fig. 8 or Fig. 9 to examine the pressure effect on oxidation kinetics. Plotting $[(x_1/x) - 2\ln(x)]$ versus $\ln(p)$ for a given level of oxidation time (t) should yield a straight line, which provides a slope as $-y$. Both sign and value of y can be used to verify the rate-determining reaction during water vapour interaction with aluminium surfaces.

Fig. 10 represents the oxide film thickness data replotted in the form $[(x_1/x) - 2\ln(x)]$ versus $\ln(p)$, using x_{rel} in place of x and x_1 estimated from Fig. 8, for the levels of oxidation time from very beginning, several minutes, to longer exposure, up to 60 min. From Fig. 10, it is evident that as the exposure time increases the experimental data tend to fall on a straight line. The slope of the linear regression line for thickness data after 60 min exposure data was estimated as -0.36, i.e. $y = 0.36$; this y value is very close to the theoretical value of 3/8, i.e. slope of the dashed line in Fig. 10, which corresponds to the oxidation kinetics with pressure dependence determined by surface reaction (14), i.e. the formation of metal vacancies at oxide film/gas interface. In consequence, the metal vacancies can be postulated as dominant defects in the oxide overlayer on aluminium surfaces. It should be noted that if the other type of defects, aluminium interstitial Al_i or oxygen vacancy V_O, were the major defect in aluminium oxide, the coefficient y would be $-3/8$ and $-1/3$, respectively. The presence of an oxygen interstitial, O''_i, in the network of aluminium oxide is rather unlikely because of the high reactivity of aluminium with oxygen and the presence of hydrogen atoms, which may be a product of the hydrolysis or oxidation reaction; else, the hydroxyl groups in interstitial positions, OH'_i, will not be the case because the value of coefficient y would have to be 1/2. On the other hand, if the pressure effect is limited to reactions (12) and (13) only, it would result in a linear dependence of the oxide thickness on water vapour pressure p. Also, if the electrostatic field is assumed to be uniform across the oxide film (i.e. not as Cabrera–Mott's assumption, $F = V/x$) and determined by a surface concentration of ionised ad-atoms only, c_{ad}, $F = c_{ad}/(\kappa\epsilon_0)$, κ and ϵ_0 are the dielectric and permittivity constants, it would result in linear, not inverse logarithmic as observed, kinetics of oxidation [from Eq. (9)].

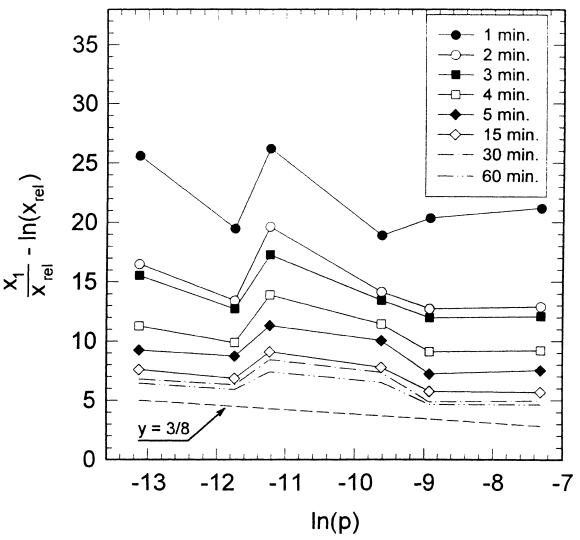

Fig. 10. The pressure dependence of growth of oxide films on aluminium surfaces: the relative thickness of oxide films as a function of pressure in the form of Eq. (15) with x_1 estimated from Fig. 8. The dashed line represents a slope of 3/8, which is the theoretical value determined for a pressure dependence of oxide growth controlled by surface reaction (14) (see text).

4. Conclusions

The effects of pressure on the interaction of water vapour with clean aluminium surfaces have been studied by the XPS technique. Detailed analy-

sis of our previous results issuing from the three-way PARAFAC technique has revealed details on the structure of the oxide overlayer as well as the mechanisms governing the oxidation kinetics. It has been shown that the oxidation kinetics can be described by the inverse logarithmic law in all studied pressures ranging from 2.0×10^{-6} to 6.5×10^{-4} Pa. The pressure effect confirms the role of a precursor for hydroxyl groups in the interaction of water vapour with aluminium surfaces. As pressure increases, the conversion of chemisorbed hydroxyl groups to oxide lattice becomes the rate-determining process, which results in an accumulation of chemisorbed hydroxyl groups on the metal surface. Thus, an increase of water vapour pressure results in larger amounts of hydroxyl groups and chemisorbed hydrogen atoms involved in the growth of oxide films. Therefore, different oxide structures develop under different exposure pressures. The pressure effect has shown also that the oxidation rate is controlled by formation reaction of metal vacancies at the oxide film/gas interface. As a result, in the thin aluminium oxide films the metal vacancies are the dominant defects, which are the main carriers in the field-driven transport of matter through the oxide films.

Acknowledgements

The authors wish to thank Alcan Aluminum Ltd. for supplying samples used in this study. T.D. also acknowledges the help of Surface Science Western of The University of Western Ontario for financial assistance.

References

[1] R.S. Alwitt, in: J.W. Diggle, A.K. Vijh (Eds.), Oxide and Oxide Films Vol. 4, Marcel Dekker, New York, 1976, p. 169.
[2] I.P. Batra, L. Kleinman, J. Electron Spectrosc. Relat. Phenom. 33 (1984) 175 and references cited therein.
[3] J.C. Fuggle, L.M. Watson, D.J. Fabian, S. Affrossman, Surf. Sci. 49 (1975) 61.
[4] F.J. Szalkowski, Chem. Phys. 77 (1982) 5224.
[5] I.E. Crowell, J.G. Chen, D.M. Hercules, J.T. Yates Jr., J. Chem. Phys. 86 (1987) 5804.
[6] C.F. McConville, D.L. Seymour, D.P. Woodruff, S. Bao, Surf. Sci. 188 (1987) 1.
[7] I. Olefjord, H.J. Mathieu, P. Marcus, Surf. Interface Anal. 15 (1990) 681.
[8] S.J. Bushby, B.W. Callen, K. Griffiths, F.J. Esposto, R.S. Timsit, P.R. Norton, Surf. Sci. 298 (1993) L181.
[9] I. Olefjord, A. Nylund, Surf. Interface Anal. 21 (1994) 290.
[10] E. McCafferty, J.P. Wightman, Surf. Interface Anal. 26 (1998) 549.
[11] N. Cabrera, N.F. Mott, Rep. Progr. Phys. 12 (1948) 163.
[12] D.D. Eley, P.R. Wilkinson, Proc. Roy. Soc. London, Ser. A 254 (1959) 327.
[13] G. Dorey, Surf. Sci. 27 (1971) 311.
[14] G.L. Hunt, I.M. Ritchie, J. Chem. Soc., Faraday Trans. I 68 (1972) 1413.
[15] W.H. Krueger, S.R. Pollack, Surf. Sci. 30 (1972) 263.
[16] V.K. Agarwala, T. Fort Jr., Surf. Sci. 45 (1974) 470.
[17] V.K. Agarwala, T. Fort Jr., Surf. Sci. 48 (1975) 527.
[18] R.Z. Bachrach, G.V. Hansson, R.S. Bauer, Surf. Sci. 109 (1981) L560.
[19] Yu.B. Makarychev, A.G. Akimov, Poverkhnost 12 (1988) 94.
[20] T. Fort Jr., R.L. Wells, Surf. Sci. 32 (1972) 543.
[21] T. Do, N.S. McIntyre, Surf. Interface Anal., (1999) in press.
[22] D.A. Shirley, Phys. Rev. B 5 (1972) 4709.
[23] T. Do, N.S. McIntyre, R.A. Harshman, M.E. Lundy, S.J. Splinter, Surf. Interface Anal. 27 (1999) 618.
[24] C.J. Powell, in: N.S. McIntyre (Ed.), Quantitative Surface Analysis of Materials, ASTM Publication 643, ASTM, Philadelphia, PA, 1978, p. 5.
[25] R.A. Harshman, UCLA Working Paper Phonet. 16 (1970) 1.
[26] J.D. Carroll, J. Chang, Psychometrika 35 (1970) 283.
[27] M. Gupta, J.P. Burger, J. Physique 41 (1980) 1009.
[28] J. Paul, F.M. Hoffmann, J. Phys. Chem. 90 (1986) 5321.
[29] J. Igalson, J.G. Adler, Phys. Rev. B 28 (1983) 4970.
[30] S. Gauthier, S. de Cheveigné, J. Klein, M. Belin, Phys. Rev. B 29 (1984) 1748.
[31] P.A. Thiry, J.J. Pireaux, M. Liehr, R. Caudano, J. Vac. Sci. Technol. A 3 (1985) 1439.
[32] J. Paul, Phys. Rev. B 37 (1988) 6164.
[33] T. Tsuchida, H. Takahashi, J. Mater. Res. 9 (1994) 2919.
[34] T.A. Carlson, Surf. Interface Anal. 4 (1982) 125.
[35] D.R. Lide (Ed.), CRC Handbook of Chemistry and Physics, 75th edn., CRC Press, Cleveland, OH, 1994/1995.
[36] B.R. Strohmeier, Surf. Interface Anal. 15 (1990) 51.
[37] S. Tanuma, C.J. Powell, D.R. Penn, Surf. Interface Anal. 17 (1991) 911.
[38] S. Tanuma, C.J. Powell, D.R. Penn, Surf. Interface Anal. 17 (1991) 927.
[39] V.A. Fomichev, A.S. Parobets, Opt. Spectrosc. 21 (1966) 419.
[40] H.-J. Hagemann, W. Gudat, C. Kunz, J. Opt. Soc. Am. 65 (1975) 742.
[41] T. Do, S.J. Splinter, C. Chen, N.S. McIntyre, Surf. Sci. 387 (1997) 192.
[42] K. Hauffe, B. Ilschner, Z. Elektrochem. 58 (1954) 382.
[43] F.A. Kröger, H.J. Vink, Solid State Phys. 3 (1956) 307.
[44] Yu.F. Zhukovkii, E.P. Smirnov, A.K. Lokenbakh, Russ. J. Phys. Chem. 64 (1990) 1825.